Open access • Journal Article • DOI:10.1103/PHYSREVA.74.023404

Creation and control of a single coherent attosecond xuv pulse by few-cycle intense laser pulses — Source link

Juan J. Carrera, Xiao-Min Tong, Shih-I Chu

Institutions: University of Kansas, University of Tsukuba

Published on: 08 Aug 2006 - Physical Review A (American Physical Society)

Topics: Attosecond, Carrier-envelope phase, Pulse (physics), High harmonic generation and Spectral density

PHYSICAL REVIEW A **74**, 023404 (2006)

Creation and control of a single coherent attosecond xuv pulse by few-cycle intense laser pulses

Juan J. Carrera,[1] X. M. Tong,[2,3] and Shih-I Chu[1]
[1]*Department of Chemistry, University of Kansas and Kansas Center for Advanced Scientific Computing, Lawrence, Kansas 66045 USA*
[2]*Institute of Materials Science, Graduate School of Pure and Applied Sciences, University of Tsukuba, 1-1-1 Tennodai, Tsukuba, Ibaraki 305-8573, Japan*
[3]*Center of Computational Sciences, University of Tsukuba, 1-1-1 Tennodai, Tsukuba, Ibaraki 305-8577, Japan*

(Received 17 March 2006; published 8 August 2006)

We present *ab initio* quantum and classical investigations on the production and control of a single attosecond pulse by using few-cycle intense laser pulses as the driving field. The high-harmonic-generation power spectrum is calculated by accurately and efficiently solving the time-dependent Schrödinger equation using the time-dependent generalized pseudospectral method. The time-frequency characteristics of the attosecond xuv pulse are analyzed in detail by means of the wavelet transform of the time-dependent induced dipole. To better understand the physical processes, we also perform classical trajectory simulation of the strong-field electron dynamics and electron returning energy map. We found that the quantum and classical results provide complementary and consistent information regarding the underlying mechanisms responsible for the production of the coherent attosecond pulse. For few-cycle (5 fs) driving pulses, it is shown that the emission of the consecutive harmonics in the supercontinuum cutoff regime can be synchronized and locked in phase resulting in the production of a coherent attosecond pulse. Moreover, the time profile of the attosecond pulses can be controlled by tuning the carrier envelope phase.

DOI: 10.1103/PhysRevA.74.023404 PACS number(s): 42.50.Hz, 32.80.Wr, 42.65.Ky, 42.65.Re

I. INTRODUCTION

In the last several years, there has been considerable interest in the development of attosecond metrology. In particular, it has been experimentally demonstrated that attosecond laser pulses can be produced by means of the process of high-order harmonic generation (HHG) in rare gases [1–8]. For example, isolated pulses were produced via spectral selection of a few harmonics in the cutoff regime that are in phase [2,4–6]. By careful amplitude and phase control of ten consecutive plateau harmonics, a train of 170 attosecond pulses has also been recently generated [7]. In general, using few-cycle driving pulses, the harmonic emission process can be confined to within a single optical cycle, so that single coherent subfemtosecond or attosecond pulses can be generated [5,6]. In the case of multicycle driving pulses, the attosecond pulse train, with a discrete spectrum containing odd harmonics of the incident radiation, can be produced [3,8].

As the interaction time between the driving laser field and atoms is confined to merely a few optical cycles, the evolution of nonlinear light matter interactions are very sensitive to the carrier envelope phase (CEP), rather than to the fundamental angular frequency of the incident radiation. Experiments have shown that short pulses with stable CEP allows one to control the electronic motion [9].

Radiation emitted by many-cycle pulses may not be synchronized on an attosecond time scale, particularly in the plateau region, hence limiting the x-ray pulse duration [10]. This intrinsic harmonic chirp can be modified by using an external chirp to the driving pulse [11]. Moreover, the phase difference between consecutive harmonics can be measured by a technique called reconstruction of attosecond beating by interference of two-photon transition (RABITT) [8]. The effect of the CEP on the phase of the harmonics has been experimentally measured [12].

In this paper, we present a detailed *ab initio* quantum and semiclassical investigations of the creation and control of a single attosecond laser pulse by means of intense few-cycle laser pulses. The time-dependent Schrödinger equation is solved accurately and efficiently by means of the time-dependent generalized pseudospectral (TDGPS) technique [13]. The time-frequency characteristics of the attosecond pulses and temporal spectra of consecutive harmonics in both plateau and cutoff regimes are analyzed by the wavelet transform of the induced dipole [14]. Note that the similar time-frequency information can be obtained by Gabor analysis [15] or the inverse Fourier transformation of the dipole in the frequency domain [16]. Our results show that quantum and classical results provide complementary and consistent information regarding the mechanisms responsible for the production of attosecond pulses. Moreover, our analysis provides physical insights regarding the CEP control of the production of attosecond laser pulses.

We will introduce our theoretical methods, both the quantum treatment and classical trajectory simulation, in Sec. II and present our simulated results and discussions in Sec. III followed by conclusions in Sec. IV.

II. THEORETICAL METHODS

A. Quantum treatment of HHG

The HHG and the attosecond xuv pulse can be studied by solving the following time-dependent Schrödinger equation (atomic units are used),

$$i\frac{\partial}{\partial t}\psi(\mathbf{r},t)=\hat{H}\psi(\mathbf{r},t)=[\hat{H}_0+\hat{V}(\mathbf{r},t)]\psi(\mathbf{r},t). \qquad (1)$$

Here, H_0 is the field-free Hamiltonian and $\hat{V}(\mathbf{r},t)$ is the time-dependent atom-field interaction. For a linearly polarized laser field ($\mathbf{F}\| z$), $\hat{V}(\mathbf{r},t)$ can be expressed

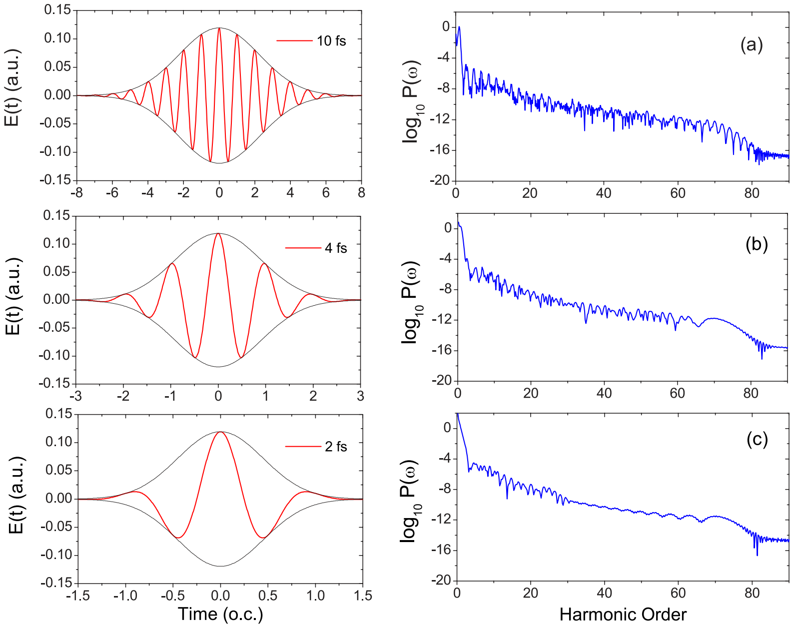

FIG. 1. (Color online) HHG power spectra of H atom in (a) 10 fs, (b) 4 fs, and (c) 2 fs pulsed laser fields. The laser parameters used are: peak intensity $I=5.0\times10^{14}$ W/cm^2, wavelength $\lambda=800$ nm, Gaussian pulse envelope, and CEP $\delta=0$. The time-dependent laser field strengths are also plotted on the left column.

$$\hat{V}(\mathbf{r},t) = -\mathbf{F}\cdot\mathbf{r}E(t) = -Fzf(t)\cos(\omega t+\delta), \tag{2}$$

with $f(t)$ being the laser field envelope, F the laser field amplitude, ω the laser frequency, and δ the carrier-envelope phase. For the hydrogen atom,

$$\hat{H}_0(\mathbf{r}) = -\frac{1}{2}\frac{d^2}{dr^2} + \frac{\hat{L}^2}{2r^2} - \frac{1}{r}. \tag{3}$$

The time-dependent Schrödinger equation can be solved accurately and efficiently by means of the TDGPS method [13] in the spherical coordinates. The TDGPS technique has been shown to be considerably more accurate and computationally more efficient than the conventional time-dependent propagation techniques using equal-spacing grid discretization [17–19]. The TDGPS numerical technique has been successfully extended to the study of field-induced Rydberg-atom high resolution spectroscopy [14] and a strong-field HHG process involving many-electron atomic and molecular systems [14,20–24].

The numerical scheme of the TDGPS method consists of two essential steps: (i) the spatial coordinates are optimally discretized in a *nonuniform* spatial grid by means of the generalized pseudospectral (GPS) technique [25]. This discretization, which uses only a modest number of grid points, is characterized by denser grids near the nuclear origin and sparser grids for larger distances. The semi-infinite domain $[0,\infty)$ of the radial coordinate r is transformed into a finite domain $x=[-1,1]$ by means of a nonlinear mapping $r=r(x)=L\frac{1+x}{1-x+\alpha}$, where L is a mapping parameter and $\alpha=2L/r_{max}$. Here r_{max} is the maximum radial distance used in the calculation. (ii) A second-order split-operator technique in the *energy* representation which allows the explicit elimination of undesirable fast-oscillating high-energy components is used for the efficient time propagation of the wave function [13],

$$\psi(\mathbf{r},t+\Delta t) \simeq \exp(-i\hat{H}_0\Delta t/2)\times\exp[-i\hat{V}(r,\theta,t+\Delta t/2)\Delta t] \times \exp(-i\hat{H}_0\Delta t/2)\psi(\mathbf{r},t) + O(\Delta t^3) \tag{4}$$

The unitarity of the wave function is automatically preserved by Eq. (4) and the norm of the field-free wave function is preserved to at least ten digits of accuracy during the time propagation. Having determined the time-dependent wave function $\psi(\mathbf{r},t)$, we can then calculate the time-dependent induced dipole acceleration as follows:

$$d_A(t) = \langle\psi(\mathbf{r},t)| -\frac{z}{r^3} + Ff(t)\cos(\omega t+\delta)|\psi(\mathbf{r},t)\rangle, \tag{5}$$

and the HHG power spectra as follows:

$$P_A(\omega) = \left|\frac{1}{t_f-t_i}\frac{1}{\omega^2}\int_{t_i}^{t_f} d_A(t)e^{-i\omega t}dt\right|^2. \tag{6}$$

We have adopted here the induced dipole acceleration form because it can be treated accurately for our present simulation scheme, using only a modest number of grid points. Up to 70 partial waves were used to achieve the convergency of the calculation. Figure 1 shows the HHG power spectra of atomic H for three pulse durations [with the field duration equal to 10, 4, and 2 fs full width at half maximum (FWHM), respectively]. All the HHG spectra show the initial decline in the lowest order harmonics, followed by a plateau of similar amplitude harmonics, and then a sharp cutoff. The subtle difference appears near the cutoff regime. For relative longer pulses [Fig. 1(a)], the cutoff regime is distinguished by well-formed individual peak structures. As the length of the pulse decreases [Fig. 1(c)], the HHG peaks in the cutoff area are replaced by one or a few pronounced supercontinuum patterns as individual adjacent peaks begin to merge with one another. The power spectra in Fig. 1 show the change of the spectra pattern in the cutoff regime from long to ultrashort laser pulses. However, the power spectra alone do not provide the time-profile information for the HHG. Such information is important to the exploration of the mechanism responsible for the generation of the attosecond pulse. In the following subsection, we present the wavelet transform method for facilitating the time-frequency analysis.

B. Time-frequency analysis of the HHG by the wavelet transform

To investigate the detailed spectral and temporal structures of HHG, we perform a time-frequency analysis by means of the wavelet transform of the induced dipole acceleration $d_A(t)$ [14,20],

$$A(t,\omega) = \int d_A(t')\sqrt{\omega}W(\omega(t'-t))dt' \equiv d_\omega(t). \qquad (7)$$

with $W(\omega(t'-t))$ is the mother wavelet. For the harmonic emission, the natural choice of the mother wavelet is a Morlet wavelet as such,

$$W(x) = \left(\frac{1}{\sqrt{\tau}}\right)e^{ix}e^{-x^2/2\tau^2}. \qquad (8)$$

Figure 2(c) shows a representative graph of the modulus of the time-frequency profile corresponding to the laser parameters of 5-fs FWHM Gaussian laser pulse with peak intensity $I=5\times10^{14}$ W/cm^2, wavelength $\lambda=800$ nm, and $\delta=0$. The laser field and its envelope are presented in Fig. 2(a). Figure 2(b) shows the returning electron energy map which will be discussed in the next subsection. Since we are studying the attosecond xuv pulse, which is located near the cutoff regime, only harmonics from the plateau to the cutoff region are shown in the figure. At the cutoff region, starting from around the 81th harmonic peak position, we note that one isolated burst of continuous frequency at the center of the laser peak field is well resolved, giving rise to a single attosecond pulse. Since the width of the central burst is much less than 1 fs, it genuinely corresponds to the production of a single attosecond xuv pulse.

As indicated earlier [14], the continuous frequency profile is an unambiguous evidence of the existence of the bremsstrahlung radiation which is emitted by the recollision of the electron wave packet with the parent ionic core. From this wavelet analysis, we see that a single attosecond laser pulse can be created by using a few-cycle laser pulse. In the next section, we present a semiclassical analysis which describes in a more intuitive picture how the attosecond pulse is actually created.

C. Classical trajectory simulation

Emission of high-order harmonics can be qualitatively explained by the semiclassical model, suggested independently by Corkum [26] and Kulander *et al.* [19]. First, an electron tunnels through the barrier formed by the atomic Coulomb potential and the laser field at time t'. The electron then oscillates quasifreely driven by the Lorenz force and acquires kinetic energy from the laser field. The electron motion in the continuum is described classically including both the Coulomb potential of the core and the laser field. At a later time t_r, after the laser reverses its direction, the tunneling electron will be driven back to its parent ionic core by the laser field with a returning energy T.

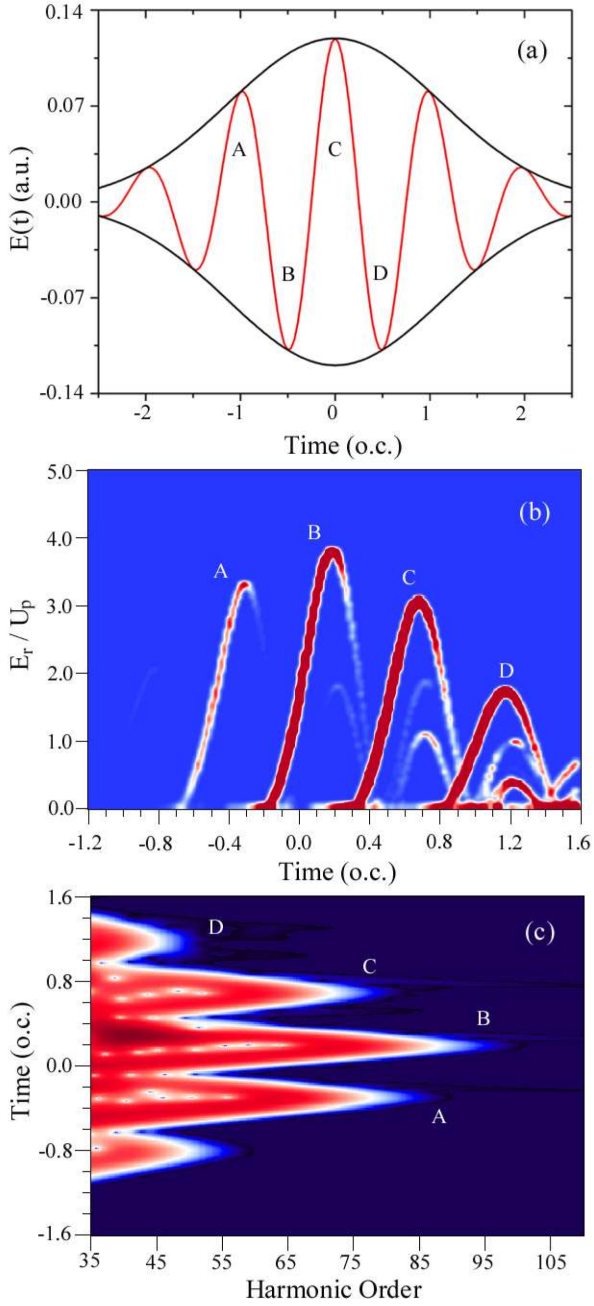

FIG. 2. (Color online) (a) Driving laser field and its envelope, (b) classical returning energy map, and (c) wavelet time-frequency profile of the HHG power spectra of hydrogen atoms driven by the short pulse laser field with peak intensity $I=5.0\times10^{14}$ W/cm^2, wavelength $\lambda=800$ nm, Gaussian time envelope, 5 fs FWHM pulse length, and CEP $\delta=0$.

The recombination times of the different electron trajectories determine the emission times of the different xuv frequencies and their possible synchronization. There are two major classes of paths which contribute to the same harmonic energy. The first trajectory is characterized by an electron returning close to one half of an optical cycle (short trajectory) and the other trajectory with returning time close to one period (long trajectory). The returning electron will emit harmonic photons by radiative recombination with the parent ionic core. The highest energy electrons are made when the electron is accelerated by a maximal of the field amplitude and thus photons with the highest energy are produced.

The probability of the electron returning at time t with returning energy E_r can be obtained from the following expression:

$$\frac{dP(E_r,t)}{dE_r dt} = \int W[|E(t')|]P(\mathbf{v})C_t(t',\mathbf{r}_0,\mathbf{v},T,t_r) \times \delta(E_r - T)\delta(t - t_r)dt'd\mathbf{v}. \qquad (9)$$

[Note that we use t_r and T which represent the returning time and returning kinetic energy for given trajectories.] Here, $W[|E(t)|]$ is the instantaneous tunneling ionization rate [27,28] which is proportional to $e^{-2\kappa^3/3E(t')}$, where $\kappa=\sqrt{2I_p}$ and I_p is the ionization potential. The tunneling ionization rate depends on the maximum field strength during the cycle and for few-cycle pulses the electron ejection rate and hence the xuv emission yield will depend on the CEP of the optical pulses [29]. The Gaussian initial velocity distributions, $P(\mathbf{v})=\frac{e^{-\mathbf{v}^2/v_0^2}}{v_0^3\sqrt{\pi^3}}$, are considered along the direction of the electric field (z direction) and in the perpendicular plane of the field [30]. Here $v_0=\sqrt{|E(t')|/\kappa}$. Such an ensemble reproduces the electron's velocity as it newly emerges from the instantaneous barrier at tunneling position r_0.

Each trajectory is monitored for all the approaches to the parent ion. If an electron trajectory is such that it can return to the parent ionic core at time t_r with returning kinetic energy T, the factor $C_t(t,\mathbf{r}_0,\mathbf{v},T,t_r)$ is set to 1; otherwise, the trajectory contribution to Eq. (9) is set to be zero, e.g., $C_t(t,\mathbf{r}_0,\mathbf{v},T,t_r)=0$.

Figure 2(b) shows the returning energy map by the classical trajectory simulation with the driving field depicted in Fig. 2(a). Clearly we can see that the photon emission times as shown in Fig. 2(c) are correlated with the returning time. A detailed discussion will be presented in the next section.

III. RESULTS AND DISCUSSION

A. Comparison of quantum and classical simulations

In this section we correlate the classical electron returning energy map with the quantum wavelet time-frequency spectrum. Figures 2 and 3, show respectively, the results for the δ=0 and $\delta=\pi/2$ cases. The tunneling electron wavepacket will be launched when the laser field reaches the local maximum at point A as seen in Fig. 2(a). The wave packet will then gain energy from the following peak field B and return to the parent ionic core between B and C [approximately 2/3 of optical cycle (o.c.)] as shown in Fig. 2(b). The electron wave packet launched from peak B will be accelerated by peak C and returns to the parent ionic core between C and D. Since peak B field is larger than that of peak A, the returning electron yield is high for B, but the returning electron energy is lower than that of A. The red regions as seen in Fig. 2(b) denote a larger number of trajectories with a given velocity than those of white regions. It is also likely that the trajectories revisit the parent ion more than once before recombination. However, these contributions are only relevant in the low-energy region. On the other hand, electronic trajectories with short return times (less than half of an optical period), significantly contribute to the cutoff spectral region [31], and hence to the production of attosecond pulses.

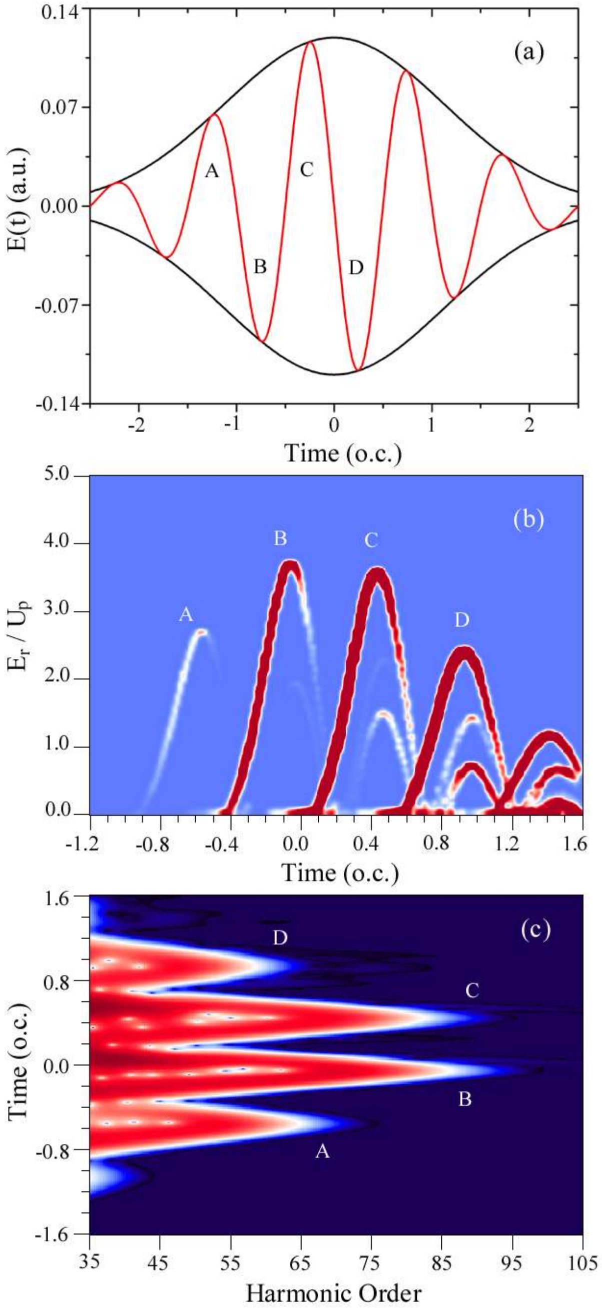

FIG. 3. (Color online) Same as Fig. 2 but for $\delta=\pi/2$.

Recollision of the electron with its parent ion may trigger several processes, including secondary electron emission, excitation of bound electrons, and emission of an energetic attosecond pulse of (soft-x-ray) photons. Furthermore, the recollision time observed at the peak maximum of each of the semiclassical trajectories remarkably corresponds to the subfemtosecond x-ray burst observed in the wavelet analysis [Fig. 2(c)]. This indicates that the HHG emissions are generated by a sequence of recollisions of the wave packet formed by the tunneling process near the peaks of the incident laser electric field and the core [14,32]. A single encounter generates a bremsstrahlung supercontinuum radiation with a broad width and an associated ultrashort temporal duration (the electron recollision time with the core). In other words, the bremsstrahlung supercontinuum radiation is generated within the attosecond time scale of the recollision. The bremsstrahlung cuts off at a frequency given by the maximum quiver energy of the recolliding electron [14,32].

The quantum and classical simulations provide consistent and complementary information regarding the mechanism for the creation of the attosecond xuv. As we illustrate in Fig. 2, the attosecond xuv pulse created in the few-cycle pulsed laser field is due to the electron tunneling out when the laser field reaches *A* peak and bounced back by the following field peak *B* and recombined with the parent ionic core later on. The cutoff energy is determined by the peak strength *B* and the yield is determined by the field strength of peak *A*. If we change the CEP, we will change the relative strength of peaks *A* and *B*. The final attosecond xuv pulse will then be modified. Figure 3 shows the simulation results similar to Fig. 2 but with $\delta=\pi/2$. For this case, we see there are two main bursts of similar intensity as opposed to the case of $\delta=0$, corresponding to the creation of two attosecond pulses.

B. Effect of CEP on the generation of attosecond pulses

To explore the effect of CEP on the formation of attosecond pulses, we investigate the time profiles of harmonics near the cutoff obtained from the wavelet time-frequency analysis. In Figs. 4(a) and 5(a), we first show the HHG power spectrum of atomic H driven by a laser field with peak intensity $I=5\times10^{14}\ \mathrm{W/cm^2}$, wavelength $\lambda=800$ nm, 5 fs FWHM, Gaussian pulse, for CEP $\delta=\pi/2$ and $\delta=0$, respectively. Figures 4(b) and 5(b) show the corresponding time profiles of a group of consecutive harmonics located close to the cutoff region for $\delta=\pi/2$ and $\delta=0$, respectively. The time profiles of the 71th to 83th harmonic orders for $\delta=\pi/2$ are shown in Fig. 4(b). We note that the dipole time profiles exhibit two peaks of similar intensity located at two different emission times which can be related to the instances *B* and *C*, respectively, shown in Fig. 3(c). On the other hand, in the case of $\delta=0$ [Fig. 5(b)], and for harmonics 77th to 87th orders, there is only one major peak profile whose maximum occurs at time *B* shown in Fig. 2(c). We note that within each group peak profile, the peak intensity as well as the width in time of each individual harmonic burst decreases accordingly as harmonics approach the end of the cutoff region. Each harmonic profile is imbedded within the next one as in Russian nesting dolls. The emission of all the consecutive harmonics in the cutoff, provided that they have similar coherent properties, can in principle be superimposed with each other to produce a stronger radiation emission. In other words, synchronization of a given range of harmonics can take place provided that each individual harmonic has similar dynamical phase $\varphi[\omega_q(t_e)]$ (also called the spectral phase) during the emission process. Note that the dipole time profile at harmonic frequency ω_q ($=q\omega$), dynamical phase, and recollision time (t_e) are related to each other by the following expression [14]:

$$d_{\omega_q}(t_e)=|d_{\omega_q}(t_e)|e^{-i(\omega_q t_e+\varphi[\omega_q(t_e)])}. \tag{10}$$

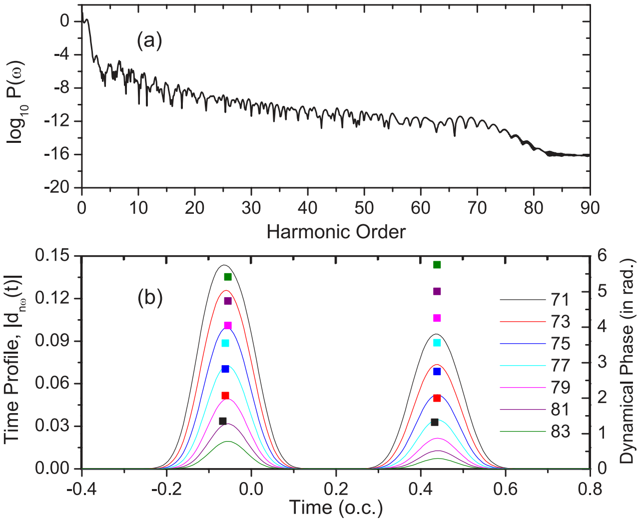

FIG. 4. (Color online) (a) HHG power spectrum for hydrogen atoms driven by a few-cycle laser field for $\delta=\pi/2$. Laser parameters are the same as those in Fig. 3. (b) Dipole time profiles of consecutive harmonics near the cutoff. Also shown are their corresponding dynamical phases, denoted as square dots, at the two "peak" emission times.

To determine the synchronization character of the emitted radiation, we compute the dynamical phase $\varphi[\omega_q(t_e)]$ from the wavelet analysis of the induced dipole acceleration, Eq. (10). The calculated dynamical phases for a group of consecutive harmonics are displayed (and denoted by small

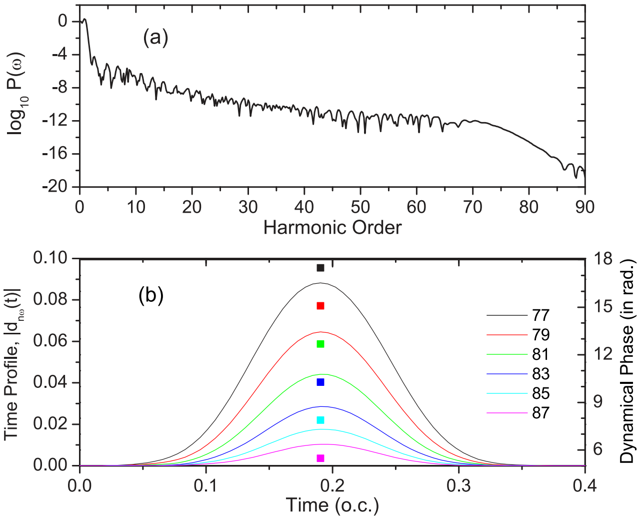

FIG. 5. (Color online) Same as Fig. 4 but for $\delta=0$.

squares) in Fig. 4(b) and Fig. 5(b), respectively, for $\delta=\pi/2$ and $\delta=0$. The peak emission times, t_e, represents where the maxima of the dipole time profile occurs, and semiclassically is interpreted as the electron-ion recollision (or recombination) times [14]. Note that the emission time from each individual harmonic does not significantly vary over time from harmonic to harmonic, indicating that all these harmonics are emitted virtually at the same instance and synchronization is achieved.

In addition, since the time profiles of the superimposed harmonics are very uniform among themselves, this implies that the harmonics are phase locked. If the harmonics were not phase locked, the corresponding time profiles could in principle exhibit irregular patterns such as multiple peaks per half cycle. Here phase locking does not mean that the harmonic components have the same phase, but rather that the phase difference $\Delta\varphi$ between neighboring harmonics remains constant [33–35].

Our calculations demonstrate that $\Delta\varphi$ between two adjacent harmonics q and $q+2$, for a given peak, is indeed nearly constant as shown in Figs. 4(b) and 5(b). For instance, in the case of $\delta=0$, the dynamical phase difference between two adjacent harmonics for the peak appearing near the 0.2 o.c. remains constant at $\Delta\varphi=2.40\pm0.01$ radians, as seen in Fig. 5(b). In the case of $\delta=\pi/2$, the phase difference for both peaks keeps unvarying at $\Delta\varphi=0.71\pm0.01$ radians. Moreover, as a consequence of the limited pulse duration, explained in [10], we can estimate the emission time from Eq. (10), to be

$$t_e=\frac{\Delta\varphi}{2\omega}. \tag{11}$$

IV. CONCLUSIONS

In conclusion, we have presented a fully *ab initio* quantum investigation and classical trajectory simulation of the creation and coherent control of a single attosecond laser pulse. The time-dependent Schrödinger equation describing the interaction of the H atoms with intense few-cycle laser pulses is solved accurately by means of the time-dependent generalized pseudospectral method. Detailed time-frequency analysis of the dipole time profile of the cutoff harmonics is performed by means of the wavelet transform of the induced dipole acceleration. It is shown that quantum and classical results provide complementary and consistent information regarding the mechanisms for the production of attosecond laser pulses. For few-cycle (5 fs) driving pulses, we found that the emission of the consecutive harmonics in the supercontinuum cutoff regime can be synchronized and locked in phase, resulting in the production of coherent attosecond pulses. Moreover, the time-frequency profile of the attosecond laser pulses can be controlled by tuning the CEP.

ACKNOWLEDGMENTS

This work was supported by the Chemical Sciences, Geosciences and Biosciences Division of the Office of Basic Energy Sciences, Office of Science, U.S. Department of Energy, and by NSF. We acknowledge the Kansas Center for Advanced Scientific Computing for the support of supercomputer time.

---

[1] M. Drescher, M. Hentschel, R. Kienberger, G. Tempea, Ch. Spielmann, G. A. Reider, P. B. Corkum, and F. Krausz, Science **291**, 1923 (2001).
[2] M. Hentschel, R. Kienberger, Ch. Spielmann, G. A. Reider, N. Milosevic, T. Brabec, P. Corkum, U. Heinzmann, M. Drescher, and F. Krausz, Nature (London) **414**, 509 (2001).
[3] P. Agostini and L. F. DiMauro, Rep. Prog. Phys. **67**, 813 (2004).
[4] R. Kienberger, M. Hentschel, M. Uiberacker, Ch. Spielmann, M. Kitzler, A. Scrinzi, M. Wieland, Th. Westerwalbesloh, U. Kleineberg, U. Heinzmann, M. Drescher, and F. Krausz, Science **297**, 1144 (2002).
[5] R. Kienberger *et al.*, Nature (London) **305**, 1267 (2004).
[6] I. P. Christov, M. M. Murnane, and H. C. Kapteyn, Phys. Rev. Lett. **78**, 1251 (1997).
[7] R. Lopez-Martens *et al.*, Phys. Rev. Lett. **94**, 033001 (2005).
[8] P. M. Paul, E. S. Toma, P. Breger, G. Mullot, F. Auge, P. Balcou, H. G. Muller, and P. Agostini, Science **292**, 1689 (2001).
[9] A. Baltška, Th. Udem, M. Uiberacker, M. Hentschel, E. Goulielmakis, Ch. Gohle, R. Holzwarth, V. S. Yakovlev, A. Scrinzi, T. W. Hänsch, and F. Krausz, Nature (London) **421**, 611 (2003).
[10] Y. Mairesse, A. de Bohan, L. J. Frasinski, H. Merdji, L. C. Dinu, P. Monchicourt, P. Breger, M. Kovačev, R. Taieb, B. Carre, H. G. Muller, P. Agostini, and P. Salieres, Science **302**, 1540 (2003).
[11] M. Murakami, J. Mauritsson, A. L'Huillier, K. J. Schafer, and M. B. Gaarde, Phys. Rev. A **71**, 013410 (2005).
[12] G. Sansone, E. Benedetti, J.-P. Caumes, S. Stagira, C. Vozzi, M. Pascolini, L. Poletto, P. Villoresi, S. De. Silvestri, and M. Nisoli, Phys. Rev. Lett. **94**, 193903 (2005).
[13] X. M. Tong and S. I. Chu, Chem. Phys. **217**, 119 (1997).
[14] X. M. Tong and S. I. Chu, Phys. Rev. A **61**, 031401(R) (2000); **61**, 021802(R) (2000); **64**, 013417 (2001).
[15] P. Antoine, B. Piraux, and A. Maquet, Phys. Rev. A **51**, R1750 (1995).
[16] M. B. Gaarde, P. Antoine, A. L'Huillier, K. J. Schafer, and K. C. Kulander, Phys. Rev. A **57**, 4553 (1998).
[17] M. R. Hermann and J. A. Fleck, Phys. Rev. A **38**, 6000 (1988).
[18] T.-F. Jiang and S. I. Chu, Phys. Rev. A **46**, 7322 (1992).
[19] K. C. Kulander, K. J. Schafer, and J. L. Krause, in Proceedings of the Workshop on Super-Intense Laser Atom Physics (SILAP) III, edited by P. Piraux (Plenum Press, New York) 316, 95 (1993).
[20] X. Chu and S. I. Chu, Phys. Rev. A **64**, 021403(R) (2001); **63**, 023411 (2001); **64**, 063404 (2001).
[21] X. Chu, S. I. Chu, and C. Laughlin, Phys. Rev. A **64**, 013406

(2001).
[22] Z. Zhou and S. I. Chu, Phys. Rev. A **71**, 011402(R) (2005).
[23] X. Chu and S. I. Chu, Phys. Rev. A **70**, 061402(R) (2004).
[24] J. J. Carrera, S. I. Chu, and X. M. Tong, Phys. Rev. A **71**, 063813 (2005).
[25] G. Yao and S. I. Chu, Chem. Phys. Lett. **204**, 381 (1993).
[26] P. B. Corkum, Phys. Rev. Lett. **71**, 1994 (1993).
[27] X. M. Tong and C. D. Lin, J. Phys. B **38**, 2593 (2005).
[28] M. V. Ammosov, N. B. Delone, and V. P. Krainov, Zh. Eksp. Teor. Fiz. **91**, 2008 (1986).
[29] A. de Bohan, P. Antoine, D. B. Milosevic, and B. Piraux, Phys. Rev. Lett. **81**, 1837 (1998).
[30] G. L. Yudin and M. Y. Ivanov, Phys. Rev. A **63**, 033404 (2001).
[31] G. Sansone, C. Vozzi, S. Stagira, and M. Nisoli, Phys. Rev. A **70**, 013411 (2004).
[32] M. Protopapas, D. G. Lappas, C. H. Keitel, and P. L. Knight, Phys. Rev. A **53**, R2933 (1996).
[33] P. Antoine, A. L'Huillier, and M. Lewenstein, Phys. Rev. Lett. **77**, 1234 (1996).
[34] M. B. Gaarde and K. J. Schafer, Phys. Rev. Lett. **89**, 213901 (2002).
[35] S. Kazamias and Ph. Balcou, Phys. Rev. A **69**, 063416 (2004).